Dynamics of information-awareness-epidemic-activity coevolution in multiplex networks

Jie Chen [1], Maobin Hu [2], and Jinde Cao [1,*]

[1] *School of Mathematics, Southeast University, Nanjing 210096, People's Republic of China*

[2] *School of Engineering Science, University of Science and Technology of China, Hefei 230026, People's Republic of China*

(Received 25 May 2023; accepted 20 July 2023; published 31 July 2023)

Epidemic spreading and awareness diffusion are typically driven by information exchange and physical contact generated by activities, respectively, evolving in a synergistic manner. In response to this reality, we propose a dynamic model of information-awareness-epidemic-activity coevolution on a four-layer network. Our findings reveal the presence of an optimal coupling between information contact preference and activity contact preference, which efficiently suppresses epidemic spreading. Specifically, the disease-related information should be targeted towards individuals who engage in more activities, enhancing their awareness and resistance to infection. Examining the epidemic situation, we observe that the epidemic threshold can be moderately increased with higher information levels but significantly decreased with increased activity frequency. Quantitatively, we establish that the epidemic threshold is strictly inversely proportional to the activity frequency. By integrating the microscopic Markov chain approach with the mean-field method, we provide theoretical insights into the system's state size and epidemic threshold. We derive an explicit expression for the critical combination of information level and activity frequency required to prevent epidemic outbreaks. These results are consistently supported by extensive Monte Carlo simulations on both heterogeneous scale-free multiplex networks and homogeneous Erdős-Rényi multiplex networks. This research emphasizes the crucial importance of reducing physical contact through activities as a key preventive measure against epidemics, complementing the focus on information dissemination to raise awareness.

DOI: 10.1103/PhysRevResearch.5.033065

I. INTRODUCTION

Throughout history, mankind has faced numerous epidemic outbreaks, from ancient plagues to more recent events such as SARS [1], H1N1 [2], and the ongoing influenza and COVID-19 pandemic [3,4]. The devastating impact of these epidemics on human life and society underscores the importance of research in epidemic modeling and control strategies [5–9]. Mathematical modeling and numerical simulations have become invaluable tools in understanding and predicting the spread of epidemics, particularly due to challenges in accessing real-time data. Complex network theory provides a promising framework for capturing the structural characteristics and dynamics of epidemic spread by representing individuals as nodes and their physical contacts as links within a network [10,11]. Consequently, the study of epidemic spreading within complex networks has garnered significant interest and attention in recent years [12–16].

Empirical evidence emphasizes that the significance of individual self-protection behaviors, such as wearing masks, maintaining social distance, isolating oneself when infected, and actively receiving vaccinations, in significantly reducing the risk of infection [17–19]. However, the adoption of these behaviors is often dominated by an individual's awareness of epidemics, which in turn affects the overall infection situation within the public health system. A seminal investigation conducted by Funk *et al.* [20] explored the positive impact of awareness dissemination on suppressing epidemic spreading in a host population. To gain a deeper understanding of the interplay between awareness and epidemics within specific network structures, multiplex networks have been introduced as a powerful tool for separately describing the spread of awareness and epidemics in two interconnected layers [21–23]. Building upon this, Granell *et al.* proposed a microscopic Markov chain approach (MMCA) to analyze the size of infectious outbreaks and the threshold for epidemic prevalence, capturing the evolution of epidemics influenced by the awareness process within the multiplex structure [24]. Subsequently, they extended their work to incorporate mass media in the spread of awareness, revealing the absence of a metacritical point for epidemic outbreaks [25]. As a result of these studies, the dynamical coevolution of awareness and epidemics on multiplex networks has emerged as a prominent research topic [26]. Existing works in this field primarily focus on expanding three key aspects: epidemic spreading models [27–29], awareness diffusion models [30–32], and multiplex structures [33,34]. Additionally, the differences in dynamic timescales between the awareness and epidemic layers have been found to significantly impact the infection status of the network system [35,36]. Recent attention has also

*jdcao@seu.edu.cn

turned to optimizing resource allocation induced by awareness diffusion as a means to impede the propagation of epidemics [37–39]. Interestingly, Wang *et al.* discovered that awareness dissemination can play an anomalous role, exacerbating the spread of epidemics and leading to larger infection sizes, particularly under limited protection and treatment resources [40]. These results shed light on the profound relationship between epidemics and the level of attention people pay to them.

The spread of epidemics is usually not a spontaneous process but rather occurs through physical contact between individuals engaging in various activities or events, such as eating, working, traveling, and exercising together. From a modeling perspective, Meloni *et al.* proposed a traffic-driven epidemic spreading model, where the intensity of epidemic propagation between individuals depends on the level of traffic flow. Their work demonstrates the ability to reproduce the vanishing threshold observed in scale-free (SF) networks under the classical epidemic model [41]. Along with this model, Yang *et al.* developed methods to suppress epidemic spreading by optimizing routing strategies, including local routing [42], global routing [43], and adaptive routing [44]. These strategies aim to distribute traffic flow in a way that reduces the scope and effectiveness of epidemic spreading. The driving propagation mechanism introduced by these models has garnered high praise for its practicality. More recently, we also extended the traffic-driven epidemic spreading model from single-layer networks to multilayer networks, but without considering the interference of awareness [45,46].

As another matter of fact, the diffusion of awareness is closely intertwined with the exchange of information. When an epidemic breaks out, disease-related information inundates various communication channels, both online and offline. This information is shared among individuals, leading to heightened awareness and consciousness regarding infection prevention. Consequently, individuals actively seek resources and regulate their behaviors accordingly to mitigate the risks. However, most previous studies treat information and awareness as a unified entity, propagated synchronously to all neighbors [24,31–33]. This oversimplification fails to capture the complexity of actual dynamics. On one hand, individuals do not communicate with all their neighbors simultaneously. On the other hand, the effectiveness of awareness dissemination often relies on the frequency and quantity of information exchange. Therefore, it is imperative to develop a coupling mechanism that accurately reflects the procedural nature of information-driven awareness dissemination, integrating it with the dynamics of epidemic spreading. Such an approach will enable us to systematically uncover the dynamic characteristics of epidemics in the real world.

Motivated by the aforementioned gaps, this paper focuses on the coevolution of awareness diffusion driven by information flow and epidemic spreading triggered by activity flow. This coevolution occurs within a constructed information-awareness-epidemic-activity (IAEA) coupling multiplex network model, which takes into account the elements of preferential contact in both the information layer and the activity layer. To begin, we integrate the MMCA with the mean-field method to theoretically analyze the sizes of aware individuals and infected individuals. This analysis allows us to approximately predict the epidemic threshold of the IAEA model, which is extensively validated through Monte Carlo (MC) simulations. Subsequently, we examine the effects of the combination of preferential contact in the information layer and the activity layer on the dynamic characteristics of epidemic spreading. We find that the optimal preference for information contact depends on the preference for activity contact. Specifically, when activities predominantly involve highly connected individuals, it becomes crucial to prioritize their information exchange to effectively contain epidemic outbreaks. Furthermore, we explore the effects of information flow level and activity flow frequency. The results show that increasing the level of information exchange can help suppress the epidemic, but only to a limited extent, particularly for high infection rates. However, a noteworthy discovery is that regardless of awareness interference, the outbreak threshold of an epidemic exhibits a power-law decline with increasing activity flow frequency. These valuable findings will offer theoretical guidance for governmental decision-making concerning resource allocation, dissemination of epidemic information, and implementation of static management measures to efficiently curb the spread of the epidemic.

II. INFORMATION-AWARENESS-EPIDEMIC-ACTIVITY COEVOLUTION MODEL

Our model is defined on a multiplex network that consists of four layers: the information layer, awareness layer, epidemic layer, and activity layer, as illustrated in Fig. 1(a). In this system, there are N individuals, corresponding to N nodes in each layer, with nodes connected across layers to represent different attributes of the same individual. The topology of the epidemic layer and activity layer is set to be identical since both involve offline physical contacts. To account for online communication, additional random links are introduced in the network topology of the activity and epidemic layers to form the information and awareness layers, which share the same topology. For convenience, let $\mathbb{A} = [a_{ij}]$ denote the adjacency matrix of the information and awareness layers, and the adjacency matrix of the activity and epidemic layers is represented as $\mathbb{B} = [b_{ij}]$. Next, the information-driven awareness diffusion dynamics and activity-triggered epidemic spreading dynamics will proceed in this multiplex system, simultaneously.

A. Information-driven awareness diffusion

In the information layer, messages and news are continuously generated and transmitted between individuals until they are ineffective. After the epidemic outbreak, we quantitatively assume that each individual obtains a certain amount of disease-related information, denoted as r, at each time step. A higher value of r indicates a higher level of information generation from mass media. Subsequently, each individual passes on all the information they possess to their neighbors one by one. To capture preferential communication contacts, the probability p_{ij} of individual i transmitting one piece of

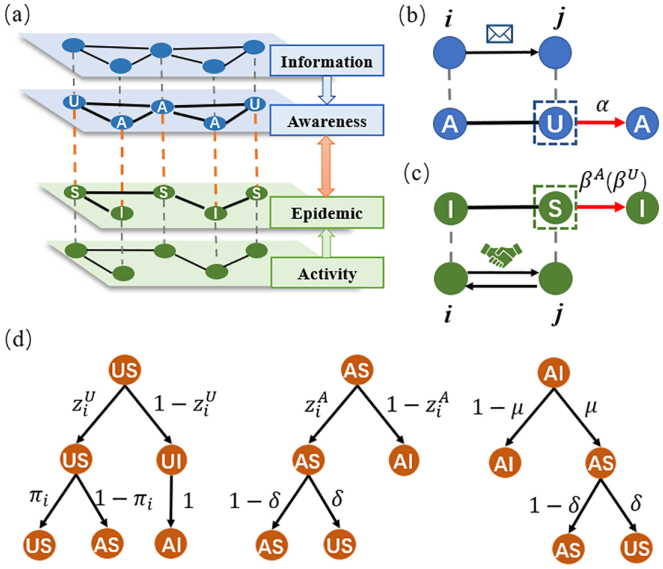

FIG. 1. Schematic illustration of the coevolution of information-driven awareness diffusion and activity-triggered epidemic spreading. (a) Four-layer multiplex network: information layer, awareness layer, epidemic layer, and activity layer. The epidemic layer and activity layer have an identical topology, while more random links are added to form the information and awareness layer with the same topology. (b) Information-driven awareness dissemination process: unaware individual j becomes aware with probability α when it receives one piece of information from an aware neighbor i. (c) Activity-triggered epidemic spreading process: susceptible individual j can be infected with probability β^{A} or β^{U}, depending on its awareness state, when it engages in an activity with an infected individual i or vice versa. (d) Transition probability trees for three states: US (unaware and susceptible), AS (aware and susceptible), and AI (aware and infected). $z_i^{\mathrm{U}}(t)$ and $z_i^{\mathrm{A}}(t)$ are the probabilities that individual i is not infected at time t when it is unaware and aware, respectively. $\pi_i(t)$ denotes the probability that an unaware individual i is not informed and does not become aware. δ and μ are the recovery rates of aware individuals and infected individuals, respectively.

information to individual j is given by

$$p_{ij} = \frac{k_j^{\chi}}{\sum_{m\in\Omega_i} k_m^{\chi}}, \tag{1}$$

where Ω_i denotes the set of neighbors of node i in the information layer and k_j is the degree of neighbor j. The parameter χ represents the preference for information exchange. Obviously, $\chi < 0$ (>0) indicates that individuals are more inclined to communicate with neighbors of smaller (larger) degrees. $\chi = 0$ corresponds to random communication. To simplify the model, the same information will not be repeatedly shared. Considering the timeliness of information, the survival time of information is set as τ time steps. Once the valid time exceeds τ, the information will be deleted from the system.

In the awareness layer, we incorporate the standard unaware-aware-unaware model [24] with the aforementioned information flow model to depict the process of information-driven awareness diffusion. In this model, all individuals are divided into two states: unaware (U) and aware (A), representing individuals who are unaware and aware of the epidemic, respectively. Normally, aware individuals have a negative inclination towards the disease-related information they possess. Therefore, when an unaware individual receive one piece of information from an aware neighbor, there is a probability α that it assimilates the information and becomes aware, as illustrated in Fig. 1(b). However, due to forgetting or negligence, an aware individual may switch back to the unaware state with probability δ at each time step.

B. Activity-triggered epidemic spreading

In the activity layer, individuals participate in various activities that involve physical contact continuously. To quantify this, we set the number of activity demands generated by each individual as λ at each time step. A larger value of λ reflects a higher frequency of individual activities. Considering the continuity of daily activities, such as multistep factory production, segmented logistics transportation, or express delivery, which involve handover operations, we assume that activities undergo κ-step transmissions between individuals from initiation to completion. For each transmission step, individual i chooses neighbor j as their activity partner with a probability q_{ij} given by

$$q_{ij} = \frac{k_j^{\theta}}{\sum_{m\in\Phi_i} k_m^{\theta}}, \tag{2}$$

where Φ_i is the set of neighbors of node i in the activity layer. The preference of physical contact generated by activity between individuals is reflected by the parameter θ. When $\theta > 0$, individuals with a higher degree have a higher probability of participating in activities. When $\theta < 0$, the occurrence of activities will concentrate on individuals with smaller degrees. When $\theta = 0$, activities are randomly conducted between individuals.

In the epidemic layer, the classical susceptible-infected-susceptible [5] model is integrated with the activity flow model from the activity layer to simulate activity-driven epidemic spreading. In this model, individuals can transition between two states: susceptible (S) and infected (I). As depicted in Fig. 1(c), when an activity takes place between a susceptible individual and an infected neighbor, which can be initiated by either the infected neighbor or the susceptible individual, the susceptible individual will become infected with a probability $\beta^{\mathrm{U}} = \beta$ if they are unaware, and with a probability $\beta^{\mathrm{A}} = \eta\beta$ ($0 \leqslant \eta \leqslant 1$) if they are in the aware state. Here, η manifests the effectiveness of self-protective behavior in the aware state. It is important to note that $\eta = 0$ and $\eta = 1$ correspond to cases where awareness can immunize individuals and has no impact on individual infection, respectively. Simultaneously, infected individuals will recover with a probability μ. Without considering the situation of asymptomatic infection, we assume that individuals will become aware of the epidemic immediately once they are infected. For simplicity, the time scale of activity-triggered activity transmission is set to be the same as that of information-driven awareness diffusion.

For ease of analysis, we summarize all the notations used in the IAEA model in Table I.

TABLE I. Summary of notations in the IAEA model.

Network layer	Notation	Description
Information	r	Information level
	τ	Information timeliness
	χ	Preference of information contact
Awareness	α	Diffusion rate of awareness
	δ	Recovery rate of aware individuals
Epidemic	β^{U}	Infection rate of unaware individuals
	β^{A}	Infection rate of aware individuals
	η	Effectiveness of awareness against infection
	μ	Recovery rate of infected individuals
Activity	λ	Activity frequency
	κ	Activity length
	θ	Preference of activity contact

III. THEORETICAL ANALYSIS

According to our IAEA coevolution model, all individuals can be categorized into three coupling states: unaware and susceptible (US), aware and susceptible (AS), and AI. To analyze the transmission dynamics and determine the epidemic threshold, we will integrate the MMCA with the mean-field method. This combined approach is of utmost importance in predicting and controlling real-world epidemics. It allows us to gain valuable insights into epidemic behavior and devise effective strategies for epidemic management.

A. Transmission dynamics

For any individual i at time t, we define the probabilities of being in the US, AS, and AI states as $\rho_i^{\mathrm{US}}(t)$, $\rho_i^{\mathrm{AS}}(t)$, and $\rho_i^{\mathrm{AI}}(t)$, respectively, where $\rho_i^{\mathrm{US}}(t)+\rho_i^{\mathrm{AS}}(t)+\rho_i^{\mathrm{AI}}(t)=1$. Additionally, we introduce the probabilistic likelihood $\pi_i(t)$, which represents the probability of unaware individual i not becoming aware, and the probabilistic likelihoods $z_i^{\mathrm{U}}(t)$ and $z_i^{\mathrm{A}}(t)$, which represent the probabilities of unaware and aware individual i not getting infected, respectively. These likelihoods can be calculated as follows:

$$\pi_i(t)=\prod_{j\in\Omega_i}[1-\alpha_{ji}(t)], \tag{3}$$

$$z_i^{\mathrm{U}}(t)=\prod_{j\in\Phi_i}\left[1-\beta_{ji}^{\mathrm{U}}(t)\right], \tag{4}$$

$$z_i^{\mathrm{A}}(t)=\prod_{j\in\Phi_i}\left[1-\beta_{ji}^{\mathrm{A}}(t)\right]. \tag{5}$$

Here $\alpha_{ji}(t)$ represents the probability that the awareness propagates from aware neighbor j to individual i in the awareness layer. Similarly, $\beta_{ji}^{\mathrm{U}}(t)$ and $\beta_{ji}^{\mathrm{A}}(t)$ are the probabilities of individual i being infected by infected neighbor j in the epidemic layer when they are unaware and aware, respectively. To calculate these probabilities, we introduce two quantities $\varphi_{ji}(t)$ and $\sigma_{ji}(t)$, representing the amount of information and activity flowing from neighbor j to individual i at time t, respectively. Regarding information-driven awareness diffusion, when an unaware individual i receives one piece of information from an aware neighbor j, the probability of remaining unaware is denoted as $1-\alpha$. Consequently, the probability of remaining unaware after receiving $\varphi_{ji}(t)$ pieces of information is given by $(1-\alpha)^{\varphi_{ji}(t)}$, while the probability of becoming aware is naturally $1-(1-\alpha)^{\varphi_{ji}(t)}$, provided that neighbor j is aware with a probability $\rho_j^{\mathrm{A}}(t)$. Thus, the calculation of $\alpha_{ji}(t)$ can be expressed as

$$\alpha_{ji}(t)=\rho_j^{\mathrm{A}}(t)\left[1-(1-\alpha)^{\varphi_{ji}(t)}\right], \tag{6}$$

where $\rho_j^{\mathrm{A}}(t)=\rho_j^{\mathrm{AS}}(t)+\rho_j^{\mathrm{AI}}(t)$. Similarly, for activity-driven epidemic spreading, a susceptible individual i can be infected by a neighbor j if individual j is infected and the activity frequency between them triggers the spread of the epidemic. This leads us to the following calculations:

$$\beta_{ji}^{\mathrm{U}}(t)=\rho_j^{\mathrm{AI}}(t)\left[1-(1-\beta^{\mathrm{U}})^{\sigma_{ji}(t)+\sigma_{ij}(t)}\right], \tag{7}$$

$$\beta_{ji}^{\mathrm{A}}(t)=\rho_j^{\mathrm{AI}}(t)\left[1-(1-\beta^{\mathrm{A}})^{\sigma_{ji}(t)+\sigma_{ij}(t)}\right], \tag{8}$$

where $\sigma_{ji}(t)+\sigma_{ij}(t)$ represents the sum of activity flow between individual i and individual j.

To accurately analyze the epidemic dynamics, it is necessary to quantitatively evaluate information and activity flows. Based on the mean-field method, we define the average amount of information reaching individual j after surviving n time steps in the information layer as φ_j^n, and the average amount of activity reaching individual j after undergoing n-step transmission in the activity layer as σ_j^n. When $n>0$, φ_j^n, and σ_j^n incorporate the information and activity transmitted by all neighbors to individual j, respectively. The recursive formulas for φ_j^n and σ_j^n can be derived as follows:

$$\begin{aligned}
\varphi_j^n &= \sum_{j_1\in\Omega_j}\varphi_{j_1}^{n-1}p_{j_1j}\\
&= \sum_{j_1\in\Omega_j}p_{j_1j}\sum_{j_2\in\Omega_{j_1}}\varphi_{j_2}^{n-2}p_{j_2j_1}\\
&= \sum_{j_1\in\Omega_j}p_{j_1j}\sum_{j_2\in\Omega_{j_1}}p_{j_2j_1}\sum_{j_3\in\Omega_{j_2}}\varphi_{j_3}^{n-3}p_{j_3j_2}\\
&\vdots\\
&= \sum_{j_1\in\Omega_j}p_{j_1j}\sum_{j_2\in\Omega_{j_1}}p_{j_2j_1}\cdots\\
&\quad\times\sum_{j_{n-1}\in\Omega_{j_{n-2}}}p_{j_{n-1}j_{n-2}}\sum_{j_n\in\Omega_{j_{n-1}}}\varphi_{j_n}^{0}p_{j_nj_{n-1}},
\end{aligned} \tag{9}$$

$$\begin{aligned}
\sigma_j^n &= \sum_{j_1\in\Phi_j}\sigma_{j_1}^{n-1}q_{j_1j}\\
&= \sum_{j_1\in\Phi_j}q_{j_1j}\sum_{j_2\in\Phi_{j_1}}\sigma_{j_2}^{n-2}q_{j_2j_1}\\
&= \sum_{j_1\in\Phi_j}q_{j_1j}\sum_{j_2\in\Phi_{j_1}}q_{j_2j_1}\sum_{j_3\in\Phi_{j_2}}\sigma_{j_3}^{n-3}q_{j_3j_2}\\
&\vdots\\
&= \sum_{j_1\in\Phi_j}q_{j_1j}\sum_{j_2\in\Phi_{j_1}}q_{j_2j_1}\cdots\\
&\quad\times\sum_{j_{n-1}\in\Phi_{j_{n-2}}}q_{j_{n-1}j_{n-2}}\sum_{j_n\in\Phi_{j_{n-1}}}\sigma_{j_n}^{0}q_{j_nj_{n-1}}.
\end{aligned} \tag{10}$$

When $n = 0$ for $j = 1, \ldots, N$, $\varphi_j^0 = r$ and $\sigma_j^0 = \lambda$ correspond to the information generation level and activity frequency of individuals. Combining with Eqs. (1) and (2), Eqs. (9) and (10) can be rewritten as

$$\begin{aligned}\varphi_j^n &= r \sum_{j_1 \in \Omega_j} \frac{k_j^\chi}{\sum_{m\in\Omega_{j_1}} k_m^\chi} \sum_{j_2 \in \Omega_{j_1}} \frac{k_{j_1}^\chi}{\sum_{m\in\Omega_{j_2}} k_m^\chi} \cdots \\ &\quad \times \sum_{j_n \in \Omega_{j_{n-1}}} \frac{k_{j_{n-1}}^\chi}{\sum_{m\in\Omega_{j_n}} k_m^\chi} \\ &\equiv r f_j(n, \chi), \end{aligned} \tag{11}$$

$$\begin{aligned}\sigma_j^n &= \lambda \sum_{j_1 \in \Phi_j} \frac{k_j^\theta}{\sum_{m\in\Phi_{j_1}} k_m^\theta} \sum_{j_2 \in \Phi_{j_1}} \frac{k_{j_1}^\theta}{\sum_{m\in\Phi_{j_2}} k_m^\theta} \cdots \\ &\quad \times \sum_{j_n \in \Phi_{j_{n-1}}} \frac{k_{j_{n-1}}^\theta}{\sum_{m\in\Phi_{j_n}} k_m^\theta} \\ &\equiv \lambda g_j(n, \theta), \end{aligned} \tag{12}$$

According to the information timeliness and activity length, we can get the average amounts of information and activity from neighbor j to individual i as follows:

$$\begin{aligned}\varphi_{ji} &= \sum_{n=0}^{\tau-1} \varphi_j^n p_{ji} = r\left[1 + \sum_{n=0}^{\tau-1} f_j(n, \chi)\right] \frac{k_j^\chi}{\sum_{m\in\Omega_i} k_m^\chi} \\ &\equiv r F_{ji}(\tau, \chi), \end{aligned} \tag{13}$$

$$\begin{aligned}\sigma_{ji} &= \sum_{n=0}^{\kappa-1} \sigma_j^n q_{ji} = \lambda\left[1 + \sum_{n=0}^{\kappa-1} g_j(n, \theta)\right] \frac{k_j^\theta}{\sum_{m\in\Phi_i} k_m^\theta} \\ &\equiv \lambda G_{ji}(\kappa, \theta). \end{aligned} \tag{14}$$

Here, $F_{ji}(\tau, \chi)$ and $G_{ji}(\kappa, \theta)$ are dependent on the multiplex network topology and known model parameters, allowing for the explicit calculation of information flow φ_{ji} and activity flow σ_{ji}. This serves as the basis for employing the MMCA to solve the probability evolution of individual states. By analyzing the transition probability trees illustrated in Fig. 1(d), we can acquire the dynamical state equations as follows:

$$\begin{aligned}\rho_i^{\mathrm{US}}(t+1) &= \rho_i^{\mathrm{US}}(t) z_i^{\mathrm{U}}(t) \pi_i(t) + \rho_i^{\mathrm{AS}}(t) z_i^{\mathrm{A}}(t) \delta \\ &\quad + \rho_i^{\mathrm{AI}}(t) \mu \delta \end{aligned} \tag{15}$$

$$\begin{aligned}\rho_i^{\mathrm{AS}}(t+1) &= \rho_i^{\mathrm{US}}(t) z_i^{\mathrm{U}}(t)[1 - \pi_i(t)] + \rho_i^{\mathrm{AS}}(t) z_i^{\mathrm{A}}(t)(1-\delta) \\ &\quad + \rho_i^{\mathrm{AI}}(t)\mu(1-\delta) \end{aligned} \tag{16}$$

$$\begin{aligned}\rho_i^{\mathrm{AI}}(t+1) &= \rho_i^{\mathrm{US}}(t)\left[1 - z_i^{\mathrm{U}}(t)\right] + \rho_i^{\mathrm{AS}}(t)\left[1 - z_i^{\mathrm{A}}(t)\right] \\ &\quad + \rho_i^{\mathrm{AI}}(t)(1-\mu). \end{aligned} \tag{17}$$

Therefore, in combination with Eqs. (3)–(17), the proportions $\rho^{\mathrm{A}}(t) = \frac{\sum_{i=1}^N [\rho_i^{\mathrm{AS}}(t) + \rho_i^{\mathrm{AI}}(t)]}{N}$ of aware individuals and $\rho^I(t) = \frac{\sum_{i=1}^N \rho_i^{\mathrm{AI}}(t)}{N}$ of infected individuals can be theoretically obtained over time.

B. Epidemic threshold

Next, we focus on the analysis of epidemic threshold for our IAEA model, which is an important performance indicator characterizing the resilience of a network system against the prevalence of a disease. As the dynamics evolve with $t \to \infty$, the state of each individual will reach stability, i.e., $\rho_i^{\mathrm{US}}(t+1) = \rho_i^{\mathrm{US}}(t) = \rho_i^{\mathrm{US}}$, $\rho_i^{\mathrm{AS}}(t+1) = \rho_i^{\mathrm{AS}}(t) = \rho_i^{\mathrm{AS}}$, and $\rho_i^{\mathrm{AI}}(t+1) = \rho_i^{\mathrm{AI}}(t) = \rho_i^{\mathrm{AI}}$ for $i = 1, \ldots, N$.

From Eqs. (7) and (8), we know that the transmission rate of epidemics is closely related to the frequency of activities between individuals. With the Taylor expansion, we can approximate $(1-\beta^{\mathrm{U}})^{\sigma_{ji}+\sigma_{ij}} \approx 1 - \beta^{\mathrm{U}}(\sigma_{ji} + \sigma_{ij})$ and $(1-\beta^{\mathrm{A}})^{\sigma_{ji}+\sigma_{ij}} \approx 1 - \beta^{\mathrm{A}}(\sigma_{ji} + \sigma_{ij})$ when the infected probability is small. Thus, Eqs. (7) and (8) can be written as

$$\beta_{ji}^{\mathrm{U}} \approx \rho_j^{\mathrm{AI}} \beta^{\mathrm{U}}(\sigma_{ji} + \sigma_{ij}), \tag{18}$$

$$\beta_{ji}^{\mathrm{A}} \approx \rho_j^{\mathrm{AI}} \beta^{\mathrm{A}}(\sigma_{ji} + \sigma_{ij}), \tag{19}$$

When the infection rate β approaches the epidemic threshold β_c, the proportion of infected individuals becomes a very small value close to 0. Thus, we assume $\rho_i^{\mathrm{I}} = \rho_i^{\mathrm{AI}} = \varepsilon_i \ll 1$ for $i = 1, \ldots, N$. Integrating this with Eqs. (18) and (19) and substituting it into Eqs. (4) and (5) yields

$$\begin{aligned} z_i^{\mathrm{U}} &\approx \prod_{j\in\Phi_i} [1 - \varepsilon_j \beta^{\mathrm{U}}(\sigma_{ji} + \sigma_{ij})] \approx 1 - \beta^{\mathrm{U}} \sum_{j\in\Phi_i} \varepsilon_j (\sigma_{ji} + \sigma_{ij}) \\ &= 1 - \beta^{\mathrm{U}} \sum_{j=1}^N b_{ji} \varepsilon_j (\sigma_{ji} + \sigma_{ij}), \end{aligned} \tag{20}$$

$$\begin{aligned} z_i^{\mathrm{A}} &\approx \prod_{j\in\Phi_i} [1 - \varepsilon_j \beta^{\mathrm{A}}(\sigma_{ji} + \sigma_{ij})] \approx 1 - \beta^{\mathrm{A}} \sum_{j\in\Phi_i} \varepsilon_j (\sigma_{ji} + \sigma_{ij}) \\ &= 1 - \beta^{\mathrm{A}} \sum_{j=1}^N b_{ji} \varepsilon_j (\sigma_{ji} + \sigma_{ij}) \end{aligned} \tag{21}$$

by ignoring the high-order terms of ε_j. Incorporating these expressions into Eq. (17), one can obtain

$$\begin{aligned} \mu \varepsilon_i &= \rho_i^{\mathrm{US}} \beta^{\mathrm{U}} \sum_{j=1}^N b_{ji} \varepsilon_j (\sigma_{ji} + \sigma_{ij}) \\ &\quad + \rho_i^{\mathrm{AS}} \beta^{\mathrm{A}} \sum_{j=1}^N b_{ji} \varepsilon_j (\sigma_{ji} + \sigma_{ij}). \end{aligned} \tag{22}$$

With the approximations $\rho_i^{\mathrm{AS}} = \rho_i^{\mathrm{A}} - \rho_i^{\mathrm{AI}} = \rho_i^{\mathrm{A}} - \varepsilon_i \approx \rho_i^{\mathrm{A}}$ and $\rho_i^{\mathrm{US}} = 1 - \rho_i^{\mathrm{AS}} - \rho_i^{\mathrm{AI}} = 1 - \rho_i^{\mathrm{A}} - 2\varepsilon_i \approx 1 - \rho_i^{\mathrm{A}}$, Eq. (22) can be simplified as

$$\sum_{j=1}^N \left\{ \left[1 - (1-\eta)\rho_i^{\mathrm{A}}\right] b_{ji}(\sigma_{ji} + \sigma_{ij}) - \frac{\mu}{\beta} e_{ji} \right\} \varepsilon_j = 0, \tag{23}$$

where e_{ji} is the element of the identity matrix $\mathbb{E}$. This equation can be transformed into a matrix expression

$$\left(\mathbb{H} - \frac{\mu}{\beta}\mathbb{E}\right)\varepsilon = 0, \tag{24}$$

where $\varepsilon = (\varepsilon_1, \varepsilon_2, \ldots, \varepsilon_N)^T$, and the element of matrix $\mathbb{H}$ is

$$\begin{aligned} h_{ji} &= \left[1-(1-\eta)\rho_i^{\mathrm{A}}\right] b_{ji}(\sigma_{ji}+\sigma_{ij}) \\ &= \lambda\left[1-(1-\eta)\rho_i^{\mathrm{A}}\right] b_{ji}[G_{ji}(\kappa,\theta)+G_{ij}(\kappa,\theta)] \\ &= \lambda l_{ji}, \end{aligned} \tag{25}$$

by combining Eqs. (13) and (14). Here, let $l_{ji} = [1-(1-\eta)\rho_i^{\mathrm{A}}]b_{ji}[G_{ji}(\kappa,\theta)+G_{ij}(\kappa,\theta)]$ as the element of matrix $\mathbb{L}$. Obviously, to make the solution of of Eq. (24) nontrivial, the minimal infection rate, known as the epidemic threshold, should be stipulated as

$$\beta_c = \frac{\mu}{\Lambda_{\max}(\mathbb{H})} = \frac{\mu}{\lambda\Lambda_{\max}(\mathbb{L})}, \tag{26}$$

where $\Lambda_{\max}(\mathbb{H})$ and $\Lambda_{\max}(\mathbb{L})$ denote the maximum eigenvalues of matrices $\mathbb{H}$ and $\mathbb{L}$, respectively. It is clear that β_c depends on several factors, including the effectiveness η of awareness, the topology b_{ji} of the epidemic layer, the activity length κ, and preference θ of activity contact, as well as the probability ρ_i^{A} of an aware individual. In quantitative terms, the epidemic threshold scales inversely with the activity frequency λ in the activity layer. Note that as β approaches β_c, the impact of the epidemic layer on the awareness layer diminishes due to $\rho_i^I \to 0$. Consequently, ρ_i^{A} can be determined independently using Eq. (A1), treating the information-driven awareness diffusion process as separate and independent from the activity-triggered epidemic propagation.

IV. RESULTS AND DISCUSSION

In this section, we conduct the extensive MC simulations to validate the MMCA equations of the IAEA coevolution model. By adopting both numerical experiments and theoretical analysis simultaneously, we explore the effects of dynamical processes of information and activity, including the selection of preference contact, flow level, and network topology, further unveiling how the information-driven awareness diffusion affects the activity-triggered epidemic spreading.

To capture the realistic characteristics of social networks, we use the heterogeneous SF network as the underlying structure to construct the IAEA multiplex network with $N = 1000$ individuals. The uncorrelated configuration model [47] is employed to generate the epidemic and activity layers, following a power-law degree distribution $P(k) = ck^{-\gamma}$ (we set $\gamma = 2.5$), constrained by $2 \leqslant k \leqslant \sqrt{N}$, and additional $M = N$ random links are added to establish the information and awareness layers. Initially, there is no epidemic, and all individuals are in an US state. Only the activity dynamic occurs on the activity layer until it reaches a stable state. Then, an epidemic is initiated by randomly selecting a fraction ρ_0 (we set $\rho_0 = 0.1$) of individuals as infection sources, who transition to an aware and infected state (AI). From this point onwards, the awareness dissemination driven by information flow and epidemic spreading triggered by activity flow coevolve over time. After a sufficiently long transition period, the system's dynamic states, including the proportions of aware individuals and infected individuals, reach stability. Average statistics are then calculated over an extended period of time to obtain reliable results.

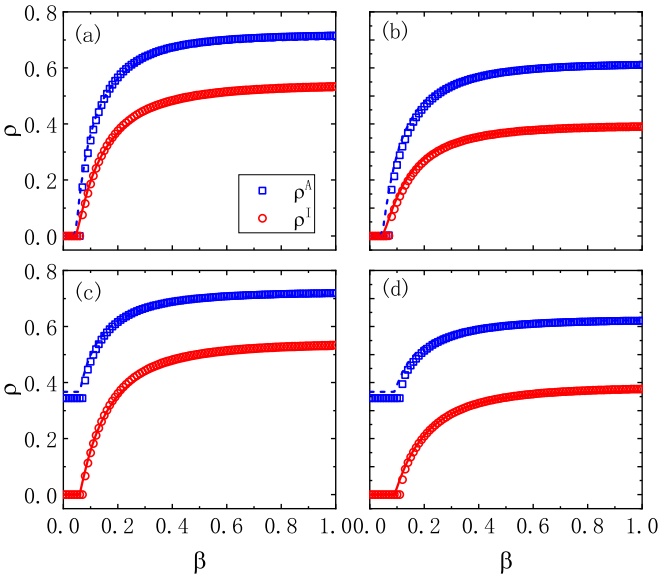

FIG. 2. Variations of the proportions ρ^{A} and ρ^{I} of aware individuals and infected individuals with the epidemic infection rate β for different combinations of the awareness diffusion rate α and awareness effectiveness η. Specifically: (a) $\alpha = 0.05$, $\eta = 0.5$; (b) $\alpha = 0.05$, $\eta = 0$; (c) $\alpha = 0.2$, $\eta = 0.5$; (d) $\alpha = 0.2$, $\eta = 0$; The data points are the results averaged over 30 MC simulations, and the corresponding color curves are the theoretical predictions of MMCA equations. Other parameters are $r = 2$, $\tau = 3$, and $\chi = 0$ in the information layer, $\delta = 0.6$ in the awareness layer, $\lambda = 3$, $\kappa = 2$, and $\theta = 0$ in the activity layer, and $\mu = 0.8$ in the epidemic layer.

A. General analysis of individual states

In this section, we present the general evolution results of the awareness and epidemic states within the IAEA model. Figure 2 shows the proportions ρ^{A} and ρ^{I} of aware individuals and infected individuals as functions of the infection rate β considering different awareness diffusion rates α and awareness effectiveness η. As β exceeds the epidemic threshold, more individuals are involved in the infection, causing ρ^{I} to rapidly increase until it reaches a nearly constant value. Simultaneously, the spread of awareness is driven by the ongoing infections, resulting in a similar evolutionary trend in ρ^{A}. It is important to note that in addition to infected individuals, the exchange of information also facilitates the spread of awareness among susceptible individuals, thus $\rho^{\mathrm{A}} = \rho^{\mathrm{AI}} + \rho^{\mathrm{AS}} = \rho^{\mathrm{I}} + \rho^{\mathrm{AS}} > \rho^{\mathrm{I}}$. By comparing four panels of Fig. 2, we can infer that a decrease in η effectively reduces the average infection of individuals, while a larger α slightly inhabits the outbreaks of epidemics by increasing ρ^{A} when β is below the epidemic threshold. Furthermore, it can be observed that the theoretical predictions based on the MMCA exhibit good consistency with the MC simulations. The mean relative errors between the two methods are 1.3%, 4.7%, 0.4%, and 2.1% for ρ^{A}, and 0.2%, 4.2%, 0.02%, and 3.2% for ρ^{I} in Figs. 2(a)–2(d), respectively. These results attest to

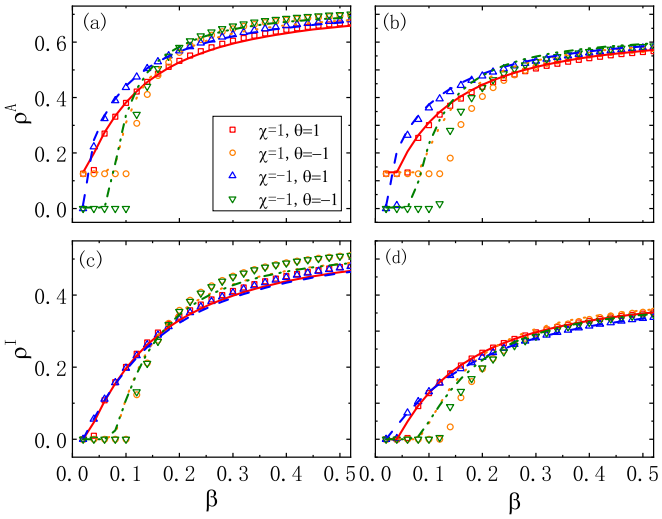

FIG. 3. Variations of the proportions ρ^{A} and ρ^{I} of aware individuals and infected individuals with the epidemic infection rate β under different combinations of the preference χ for information contact and the preference θ for activity contact, considering two scenarios of awareness effectiveness: $\eta = 0.5$ and $\eta = 0$. (a) ρ^{A} vs β for $\eta = 0.5$; (b) ρ^{A} vs β for $\eta = 0$; (c) ρ^{I} vs β for $\eta = 0.5$; (d) ρ^{I} vs β for $\eta = 0$. The data points are the results averaged over 30 MC simulations, and the corresponding color curves are the theoretical predictions of MMCA equations. Other parameters are $r = 2$ and $\tau = 3$ in the information layer, $\alpha = 0.1$ and $\delta = 0.6$ in the awareness layer, $\lambda = 3$ and $\kappa = 2$ in the activity layer, and $\mu = 0.8$ in the epidemic layer.

the validity of the dynamic analysis of awareness-epidemic coevolution on IAEA multiplex networks.

B. Effect of contact preference

Having gained a general understanding of the evolution characteristics of individual states, we now delve into the impact of contact preferences in information and activity on awareness diffusion and the spread of epidemics. Figure 3 presents the results of MC simulations and the corresponding predictions from the MMCA under different combinations of contact preferences (χ, θ). Notably, the agreement between the MMCA predictions and MC simulations remains strong across various contact preferences. However, significant differences can be observed in the changes of ρ^{A} and ρ^{I} with respect to the infection rate β for different combinations of (χ, θ). Comparing the results in Fig. 3, we find that the differences in ρ^{A} and ρ^{I} become more pronounced at lower values of β but converge at higher values of β. In Figs. 3(a) and 3(b), the initial discrepancy in ρ^{A} is attributed to the different awareness thresholds influenced by χ (see Appendix A), where α lies above the awareness threshold for $\chi = 1$ but below that for $\chi = -1$. In Fig. 3(c), the influence of θ on the evolution of ρ^{I} is evident, particularly with respect to the epidemic threshold. However, the information-driven awareness diffusion under different χ does not significantly interfere with this impact. This can be explained as follows: The activity contact preference θ plays a dominant role in determining the direction of activity flow, which directly affects the distribution of epidemics and has a significant impact on the proportion of

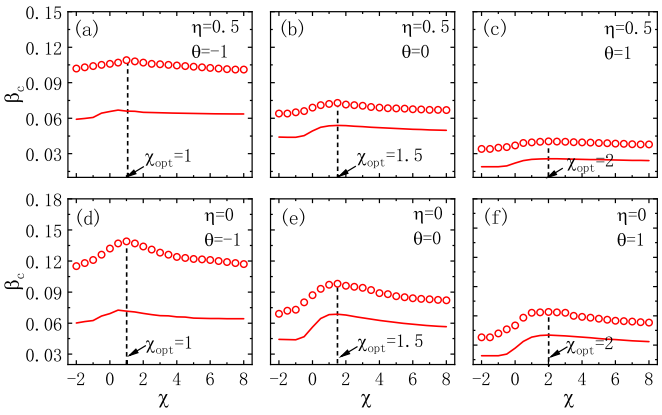

FIG. 4. Variation of the epidemic threshold β_c with the information contact preference χ under different activity contact preferences θ for different awareness effectiveness η. (a)–(c) $\theta = -1$, 0, and 1 when $\eta = 0.5$; (d)–(f) $\theta = -1$, 0, and 1 when $\eta = 0$. The data points are the results obtained by MC simulations, and the curves are the theoretical predictions by Eq. (26). Other parameters are $r = 2$ and $\tau = 3$ in the information layer, $\alpha = 0.1$ and $\delta = 0.6$ in the awareness layer, $\lambda = 3$ and $\kappa = 2$ in the activity layer, and $\mu = 0.8$ in the epidemic layer.

infected individuals ρ^{I}. In contrast, the information contact preference χ has a reduced influence on the size and distribution of aware individuals ρ^{A} as the overlap between infected and aware individuals increases with the infection rate β. Therefore, the impact of χ on ρ^{A} has a smaller influence on the epidemic size ρ^{I}. When the inhibitory effect of awareness on epidemic transmission is enhanced (e.g., by changing η from 0.5 to 0), different values of χ result in distinct epidemic thresholds, as shown in Fig. 3(d). As a result, the outbreak and spread of the epidemic are closely related to the contact preferences of both information and activity.

To gain more insight into the coevolution dynamics of IAEA, we focus on the epidemic threshold, which can be identified by leveraging the susceptibility Δ_ρ at each infection rate β in the MC simulations as follows [48]:

$$\Delta_{\rho^I} = N \frac{\langle \rho^{\mathrm{I}2} \rangle - \langle \rho^{\mathrm{I}} \rangle^2}{\langle \rho^{\mathrm{I}} \rangle}, \tag{27}$$

where $\langle \rho^{\mathrm{I}2} \rangle$ and $\langle \rho^{\mathrm{I}} \rangle$ are the ensemble averages of $\rho^{\mathrm{I}2}$ and ρ^{I} over all realizations of the MC simulation. The epidemic threshold β_c corresponds to the infection rate at which $\Delta_{\rho^{\mathrm{I}}}$ reaches a diverging peak.

Figure 4 reports the variation of epidemic threshold β_c with the information contact preference χ under different activity contact preferences θ when η is 0.5 and 0, respectively. It is easy to see that for different θ, β_c exhibits clear nonmonotonic behaviors as χ increases, with this effect being more pronounced at $\eta = 0$ compared to $\eta = 0.5$. This behavior can be explained by considering that, with the distribution of activity flow determined by a certain θ, individuals engaged in more activities also bear a higher risk of infection. By choosing an appropriate χ, more disease-related information can be disseminated to these individuals, strengthening their awareness and reducing their probability of infection, thereby raising the epidemic threshold. However, if χ is either too large or too

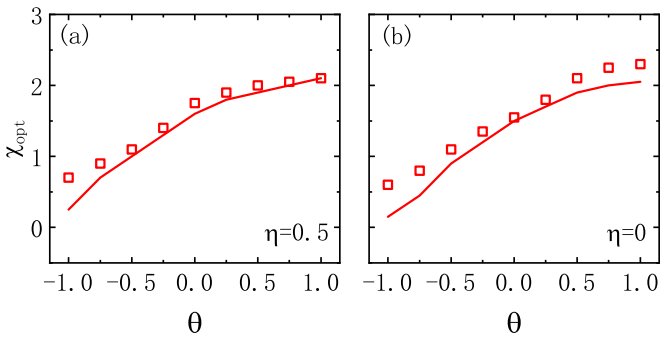

FIG. 5. Variation of the optimal information contact preference χ_{opt} with the activity contact preference θ for different awareness effectiveness η. (a) $\eta = 0.5$; (b) $\eta = 0$. The data points are the results obtained by MC simulations, and the curves are the theoretical predictions by Eq. (26). Other parameters are $r = 2$ and $\tau = 3$ in the information layer, $\alpha = 0.1$ and $\delta = 0.6$ in the awareness layer, $\lambda = 3$ and $\kappa = 2$ in the activity layer, and $\mu = 0.8$ in the epidemic layer.

small, the distribution of information flow will not match the distribution of activity flow, resulting in a mismatch between awareness diffusion and epidemic spread, which ultimately degrades the system's ability to contain the epidemic. Consequently, β_c achieves its maximum value at an optimal χ_{opt}, which varies with θ, indicating that adjusting the information contact preference based on the activity contact preference is an important way to improve the system's defense performance.

On the other hand, a smaller value of θ tends to favor individuals with small degree to engage in activities. Since the epidemic relies on them for a smaller transmission range, this preference can contribute to a larger epidemic threshold. Furthermore, the theoretical results predicted by Eq. (26) show qualitative consistency with the experimental simulations. The acceptable deviations are mainly provoked by the approximations made during solving and the neglect of dynamic correlations among network layers.

To optimize epidemic control measures, it is beneficial to identify the optimal combination (χ, θ) that produces a larger epidemic threshold. In Fig. 5, we illustrate the optimal preference χ_{opt} for information contact corresponding to different activity contact preferences θ when $\eta = 0.5$ and $\eta = 0$. Obviously, χ_{opt} keeps increasing with the increase of θ. This observation can be explained by the fact that a larger θ emphasizes activities involving individuals with higher degrees, thereby necessitating the directed dissemination of more information to enhance their awareness. In addition, the theoretical χ_{opt} based on Eq. (26) closely aligns with the numerical results, irrespective of the value of η, thereby confirming the effectiveness and reliability of our analytical approach once again. These findings provide valuable insights for designing prevention and control strategies during the epidemic period, especially when resuming work and production.

C. Effect of information and activity flows

The mutual interference between awareness and epidemics ultimately stems from the flow of information and activities. In this regard, we investigate the role of information level and

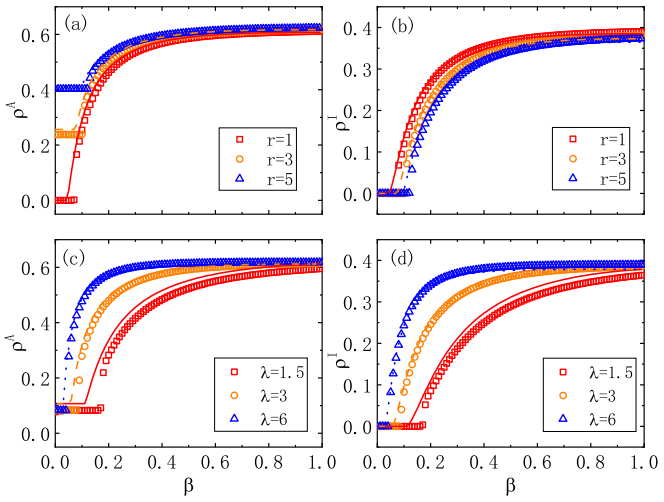

FIG. 6. Variations of the proportions ρ^A and ρ^I of aware individuals and infected individuals with the epidemic infection rate β under different information levels r and activity frequencies λ. (a) ρ^A vs β for different r; (b) ρ^I vs β for different r. Here, (c) ρ^a vs β for different λ; (d) ρ^I vs β for different λ. The data points are the results averaged over 30 MC simulations, and the corresponding color curves are the theoretical predictions of MMCA equations. Here, $\lambda = 3$ in (a) and (b), and $r = 2$ in (c) and (d). Other parameters are $\tau = 3$ and $\chi = 0$ in the information layer, $\alpha = 0.1$ and $\delta = 0.6$ in the awareness layer, $\kappa = 2$ and $\theta = 0$ in the activity layer, and $\mu = 0.8$ and $\eta = 0$ in the epidemic layer.

activity frequency, characterized separately by the parameters r and λ in the IAEA coevolution model. As shown in Fig. 6, we plot the evolution of the proportions ρ^A and ρ^I as a function of the epidemic infection rate β under different values of r and λ, respectively. The agreement between the MMCA and MC results demonstrates that our prediction analysis is robust to the flow levels of information and activity. From Figs. 6(a) and 6(b), one can observe that when β is less than β_c, a larger r leads to a significantly higher proportion ρ^A of aware individuals, thereby delaying the outbreak of the epidemic. Once β exceeds β_c, the difference in ρ^A among different r quickly subsides as β increases, resulting in a slight decrease in the proportion of infected individuals with the increase of r. However, in the case of λ, its impact is more clear in terms of the epidemic threshold and individual states. As shown in Figs. 6(c) and 6(d), the obvious increase of both ρ^A and ρ^I with increasing λ reflects the promotion of activity frequency for the spread of the epidemic. Moreover, the distinct gap in the phase transition position among different λ values indicates that an increase in activity frequency can significantly influence the outbreak of the epidemic.

To further elucidate the quantitative impact of information and activity flows, Fig. 7(a) first depicts the relationship between the epidemic threshold β_c and the information level r for different information timeliness τ. Both theoretical and numerical results demonstrate that increasing r can help improve β_c for all τ, particularly for larger τ where the effect is more pronounced. Also, a larger τ corresponds to a larger β_c, since it implies that more timely information is available to individuals, thus increasing their awareness of the epidemic. Therefore, reinforcing the dissemination of information

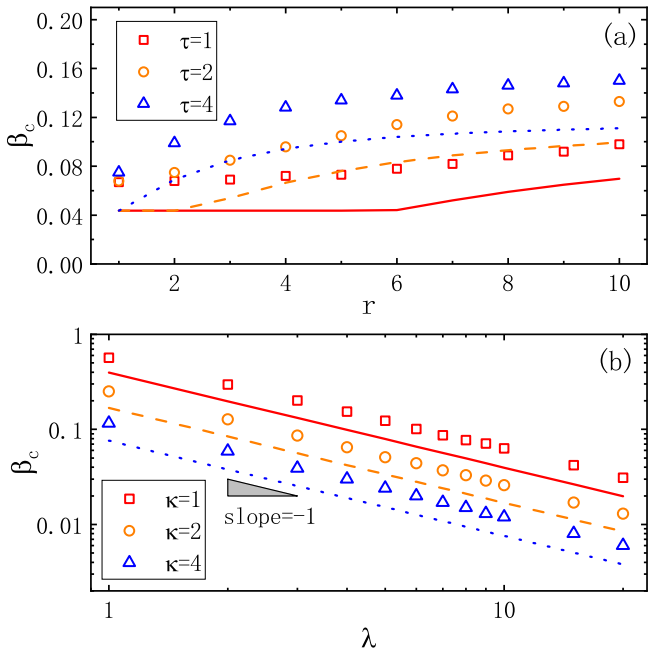

FIG. 7. Effects of the information level r and activity frequency λ on the epidemic threshold β_c. (a) β_c vs r for different information timeliness τ, where $\lambda = 3$ and $\kappa = 2$; (b) β_c vs λ for different activity lengths κ, where $r = 2$ and $\tau = 3$. The data points are the results obtained by MC simulations, and the corresponding color curves are the theoretical predictions by Eq. (26). Other parameters are $\chi = 0$ in the information layer, $\alpha = 0.1$ and $\delta = 0.6$ in the awareness layer, $\theta = 0$ in the activity layer, and $\mu = 0.8$ and $\eta = 0$ in the epidemic layer.

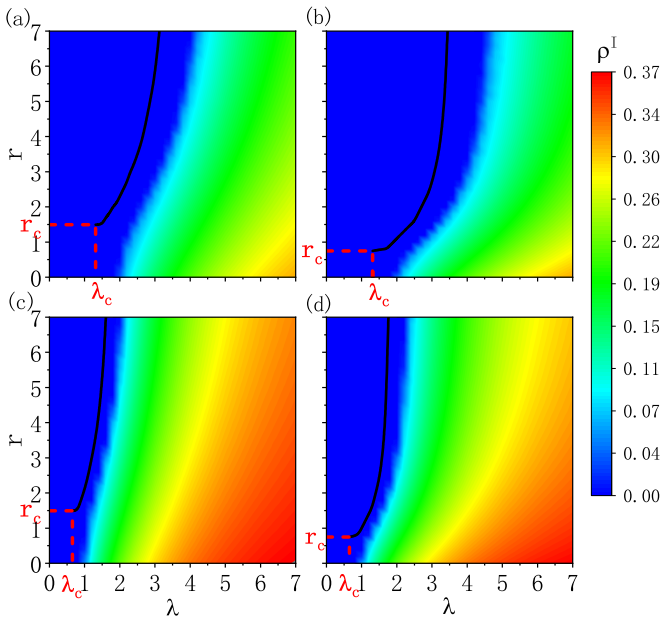

FIG. 8. Phase diagrams of ρ^{I} in the plane of the information level r and the activity frequency λ for different combinations of the awareness diffusion rate α and the epidemic infection rate β. (a) $\alpha = 0.1$, $\beta = 0.1$; (b) $\alpha = 0.2$, $\beta = 0.1$; (c) $\alpha = 0.1$, $\beta = 0.2$; (d) $\alpha = 0.2$, $\beta = 0.2$. Color-coded values of ρ_{I} are obtained by MC simulations on a 35×35 grid, and each ρ^{I} is the result averaged over 30 realizations. The black solid curves are the theoretical predictions for complete suppression of the epidemic by Eq. (28). r_c and λ_c corresponding to the red dashed lines are the critical information levels and activity frequencies determined by Eqs. (A7) and (B4), respectively. Other parameters are $\tau = 3$ and $\chi = 0$ in the information layer, $\delta = 0.6$ in the awareness layer, $\kappa = 2$ and $\theta = 0$ in the activity layer, and $\mu = 0.8$ and $\eta = 0$ in the epidemic layer.

related to epidemics is still beneficial for suppressing the spread of epidemics. Next, in Fig. 7(b), we explore the evolution of β_c under different activity lengths κ for varying activity frequencies λ. Qualitatively, it can be observed that β_c decreases significantly with the increase of λ and κ. From a quantitative standpoint, the simulation results show that β_c is strictly inversely proportional to λ, which is consistent with the theoretical analysis provided by Eq. (26). Overall, compared to the information level, the activity frequency exerts a stronger impact on the outbreak of epidemics.

To explore the coordinated control of epidemic spread through the interplay of information level and activity frequency, we examine the dynamic relationship between r and λ in Fig. 8. The proportion ρ^{I} of infected individuals is plotted as a function of r and λ for different combinations of α and β. Notably, ρ^{I} decreases with increasing α and r, while the opposite and significant changes occur with β and λ. A clear boundary can be observed, which is determined by the critical activity frequency dependent on r, distinguishing whether the epidemic has erupted. When r is small ($r < r_c$, see Appendix A), it is insufficient to drive the diffusion of awareness, and the epidemic spreading is primarily influenced by the activity flow. In this case, the variation of r does not change the critical activity frequency, denoted as λ_c (see Appendix B) for independent activity-driven epidemic spreading. However, as r increases beyond r_c, the awareness becomes prevalent in the system, suppressing the epidemic propagation and resulting in an increase in the critical activity frequency. Nevertheless, as r continues to increase, the effect of increasing the critical activity frequency becomes less significant, as the size ρ^{A} of aware individuals tends to reach a constant value [see Fig. 12(b)]. Comparing Figs. 8(c) and 8(d) with Figs. 8(a) and 8(b), we find that the increase in the critical activity frequency with r also weakens with an increase in β. While strengthening information dissemination for epidemic prevention ensures the health of the system, it allows for a certain degree of increase in activity frequency. However, this effect is limited for higher epidemic infection rates. According to Eq. (26), since the element ρ_i^{A} of the matrix $\mathbb{L}$ is related to α and r [see Eq. (A1)], the theoretical predictions for the boundary can be expressed as follows:

$$\frac{\mu}{\lambda \Lambda_{\max}(\mathbb{L}(\alpha, r))} \gtrsim \beta, \tag{28}$$

By integrating Eq. (28) with Eqs. (A7) and (B4), we can well determine the region where the information flow suppresses the outbreak of the epidemic across the activity frequency in all combinations of α and β of Fig. 8.

D. Effect of network topology

Network topology plays a pivotal role in shaping the spread and outbreak of epidemics. To this end, we first investigate the

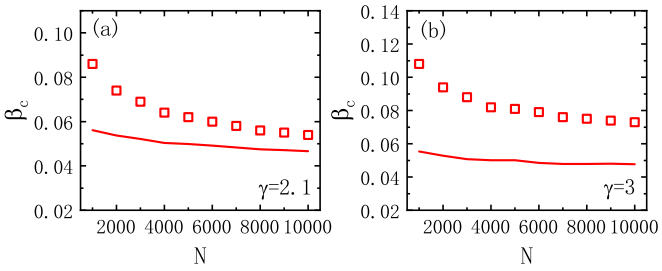

FIG. 9. Variation of the epidemic threshold β_c with the network size N for different degree distributions γ of SF multiplex networks. (a) $\gamma = 2.1$; (b) $\gamma = 3$. The data points are the results obtained by MC simulations and the curves are the theoretical predictions by Eq. (26). Other parameters are $r = 2$, $\tau = 3$, and $\chi = 0$ in the information layer; $\alpha = 0.1$ and $\delta = 0.6$ in the awareness layer; $\lambda = 3$, $\kappa = 2$, and $\theta = 0$ in the activity layer, and $\mu = 0.8$ in the epidemic layer.

dependency of the epidemic threshold on the system size for IAEA coevolution dynamics. As depicted in Fig. 9, one can observe a decreasing trend of the epidemic threshold β_c with increasing network size N for different degree distributions γ of SF multiplex networks. The theoretical predictions based on Eq. (26) are compared with the corresponding numerical results. Notably, the reduced differences between the theoretical and numerical values with increasing network size N indicate that our analytical method becomes more efficient for larger network systems. This finding suggests that finite-size effects may impact the accuracy of our theoretical predictions.

To demonstrate the generality of our analytical approach and results, we have conducted additional simulation experiments on a homogeneous random multiplex network, where the SF topology of network layers is replaced with an Erdős-Rényi (ER) random topology [49] with an average degree of $\langle k \rangle = 4$. Figure 10(a) compares the evolution of the proportion ρ^{I} of infected individuals obtained from MC simulations with the predictions of MMCA under different combinations of the preference χ for information contact and the preference θ for activity contact. We observe good agreement between the two methods, validating the effectiveness of our analytical approach across various parameter settings. Building on this, we utilize Eq. (26) to theoretically predict how the epidemic threshold β_c is affected by the preferences χ and θ on ER multiplex networks. As shown in Fig. 10(b), one can find that negative values of θ leads to larger values of β_c compared to positive θ. Similarly, β_c evolves nonmonotonically with χ for all listed θ, with an optimal $\chi \approx 2$ that maximizes the system

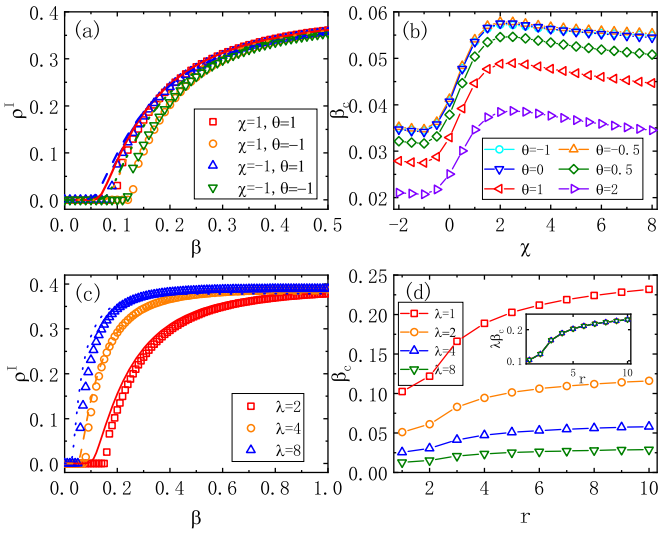

FIG. 10. IAEA coevolution dynamics on the ER multiplex network. (a) Proportion ρ^{I} of infected individuals obtained from 30 MC simulations (data points) and MMCA equations (curves) versus the epidemic infection rate β under different combinations of the preference χ for information contact and the preference θ for activity contact. (b) Epidemic threshold β_c obtained by Eq. (26) versus the preference χ for information contact under different preferences θ of activity contact. (c) Proportion ρ^{I} of infected individuals obtained from 30 MC simulations (data points) and MMCA equations (curves) versus the epidemic infection rate β under different activity frequencies λ. (d) Epidemic threshold β_c obtained by Eq. (26) versus the information levels r under different activity frequencies λ. The inset plots $\lambda\beta_c$ as a function of r for different λ. In (a) and (b), $r = 2$ and $\lambda = 3$. In (c) and (d), $\chi = 0$ and $\theta = 0$. Other parameters are $\tau = 3$ in the information layer, $\alpha = 0.1$ and $\delta = 0.6$ in the awareness layer, $\kappa = 2$ in the activity layer, and $\mu = 0.8$ and $\eta = 0$ in the epidemic layer.

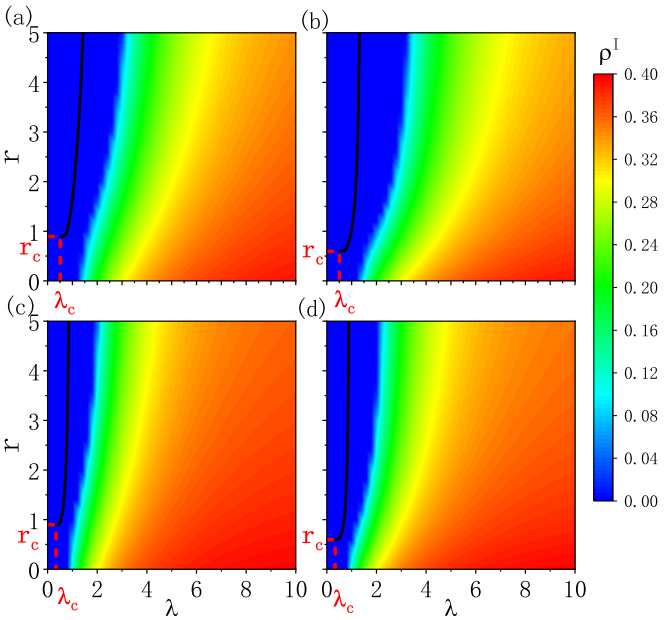

FIG. 11. Phase diagrams of ρ^{I} in the plane of the information level r and the activity frequency λ for different combinations of the awareness diffusion rate α and the epidemic infection rate β when the ER multiplex network is adopted. (a) $\alpha = 0.2$, $\beta = 0.2$; (b) $\alpha = 0.3$, $\beta = 0.2$; (c) $\alpha = 0.2$, $\beta = 0.3$; (a) $\alpha = 0.3$, $\beta = 0.3$. Color-coded values of ρ_I are obtained by MC simulations on a 50×25 grid, and each ρ^{I} is the result averaged over 30 realizations. The black solid curves are the theoretical predictions for complete suppression of the epidemic by Eq. (28). r_c and λ_c corresponding to the red dashed lines are the critical information levels and activity frequencies determined by Eqs. (A7) and (B4), respectively. Other parameters are $\tau = 3$ and $\chi = 0$ in the information layer, $\delta = 0.6$ in the awareness layer, $\kappa = 2$ and $\theta = 0$ in the activity layer, and $\mu = 0.8$ and $\eta = 0$ in the epidemic layer.

performance in defending against epidemic outbreaks. Furthermore, the effects of activity frequency λ and information level r is also explored on the ER multiplex network. From Fig. 10(c), we verify that our analytical predictions remain effective for epidemic prediction on the ER multiplex network. Subsequently, Fig. 10(d) presents the variation of the theoretical epidemic threshold β_c with r for different values of λ. The result shows that increasing λ leads to more distinct values of β_c, and an increase in r improves β_c. Moreover, the inset of Fig. 10(d) demonstrates the overlapping evolution of $\lambda\beta_c$ with r for different λ, once again clarifying the inverse relationship between the epidemic threshold and activity frequency.

To unveil the interplay between activity frequency and information level on the ER multiplex network, we examine the results of the proportion ρ^{I} of infected individuals as a function of r and λ, as well as different combinations of α and β. Figure 11 illustrates the comparison between the theoretical predictions and numerical simulations, demonstrating their qualitative agreement. Consistent with the results on the SF multiplex network, we observe that increasing the information level slightly raises the critical activity frequency and effectively reduces the infection size of individuals when an epidemic outbreak occurs. Furthermore, compared to the suppression of epidemics achieved through increased awareness diffusion, the impact of epidemic prevalence becomes more significant with an increase in the infection rate. These observations highlight the complex interplay between activity frequency and information level in controlling epidemic outbreaks on the ER multiplex network. It emphasizes the importance of finding a balance between these factors to effectively mitigate the spread of epidemics.

V. CONCLUSION

In this paper, we have introduced an IAEA coevolution dynamics model on four-layer multiplex networks, considering the preferences of information exchange and activity contact. By integrating a MMCA with mean-field approximation, we have developed a theoretical method to analyze the interplay between information-driven awareness diffusion and activity-triggered epidemic spreading. Our model and method provide insights into the dynamics of spreading processes.

In summary, we have made the following key findings. First, we have demonstrated the effectiveness of our theoretical approach through extensive MC simulations, showing good agreement between the theoretical predictions and simulation results in predicting the size of individual states and the epidemic threshold. Second, we have identified an optimal preference for information exchange that depends on the preference for activity contact, which maximizes the epidemic threshold. This highlights the importance of information reminders in strengthening individuals' self-protection awareness, particularly for those engaged in more activities. Third, we have investigated the effects of information level and activity frequency on the epidemic size and threshold. Our results indicate that increasing the information level can raise the epidemic threshold, while decreasing the activity frequency plays a crucial role in suppressing the spread of the epidemic.

We have validated our model and method on both heterogeneous SF multiplex networks and homogeneous ER random networks, and observed consistent results. Our approach captures the essential dynamics of information-dependent awareness diffusion and activity-dependent epidemic spreading, providing valuable insights for modeling and analyzing epidemic prevention strategies. The findings underscore the importance of effectively controlling information and activity flows to mitigate the spread of epidemics. Future work in this area may involve exploring the integration of resources and information to further enhance epidemic control strategies.

ACKNOWLEDGMENTS

The research was supported by the Key Project of Natural Science Foundation of China (No. 61833005), the National Key Research and Development Project of China (No. 2020YFA0714301), the Natural Science Foundation of China (No. 12072340), the Jiangsu Funding Program for Excellent Postdoctoral Talent (No. 2022ZB130), and the Project funded by China Postdoctoral Science Foundation, China (No. 2022M720727).

APPENDIX A: INDEPENDENT INFORMATION-DRIVEN AWARENESS DIFFUSION

In cases where the epidemic does not break out in the system due to a small infected rate or activity frequency, there are very few or no individuals in an infected state, which results in little interference in the dynamics of the awareness layer. Under these conditions, the information-driven awareness diffusion can be considered independent of activity-triggered epidemic spreading. By employing the MMCA, we can model the evolution of the aware state over time as follows:

$$\rho_i^{\mathrm{A}}(t+1) = \left[1-\rho_i^{\mathrm{A}}(t)\right][1-\pi_i(t)] + \rho_i^{\mathrm{A}}(t)(1-\delta), \quad \text{(A1)}$$

where the two items on the right-hand side refer to the generation of new aware individuals and the decay of individual awareness, respectively. As shown in Figs. 12(a) and 12(b), the steady proportion ρ_i^{A} of aware individuals increases with the awareness diffusion rate α and information level r. The theoretical predictions based on Eq. (A1) are consistent with the MC simulations, which provides the accessibility for Eq. (26) to accurately predict the epidemic threshold of the IAEA coevolving dynamics.

Next, we focus on the theoretical analysis of the critical information level r_c illustrated in Figs. 8 and 11. When the system approaches a stable state of awareness prevalence, we assume $\rho_i^{\mathrm{A}}(t+1) = \rho_i^{\mathrm{A}}(t) = \varepsilon_i^{\mathrm{A}} \ll 1$ for $i = 1, \ldots, N$. With the approximation $(1-\alpha)^{\varphi_{ji}} \approx 1 - \alpha\varphi_{ji}$, Eq. (6) can be rewritten as

$$\alpha_{ji} \approx \alpha\varepsilon_j^{\mathrm{A}}\varphi_{ji}. \quad \text{(A2)}$$

Substituting Eq. (A2) into Eq. (3) and omitting the high-order terms of $\varepsilon_j^{\mathrm{A}}$, we can obtain

$$\begin{aligned}\pi_i &\approx \prod_{j\in\Omega_i}\left(1-\alpha\varepsilon_j^{\mathrm{A}}\varphi_{ji}\right) \approx 1-\alpha\sum_{j\in\Omega_i}\varepsilon_j^{\mathrm{A}}\varphi_{ji} \\ &= 1-\alpha\sum_{j=1}^{N}\varepsilon_j^{\mathrm{A}}a_{ji}\varphi_{ji}.\end{aligned} \quad \text{(A3)}$$

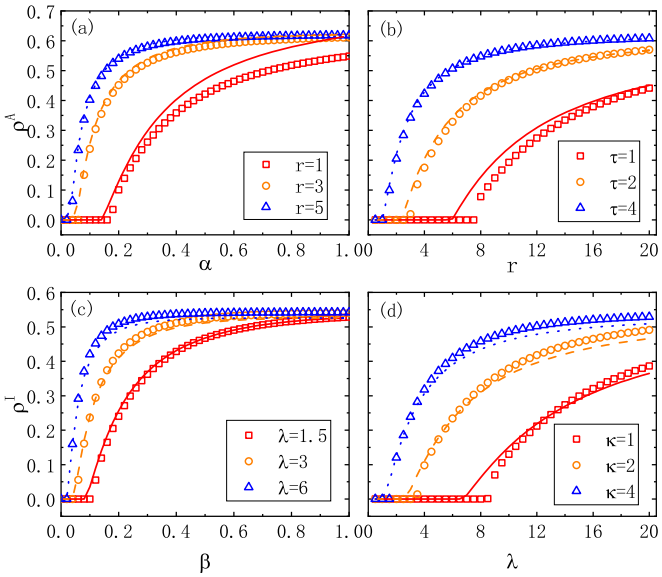

FIG. 12. Independent information-driven awareness diffusion: (a) Variation of the proportions ρ^{A} of the aware individuals with the awareness diffusion rate α for different information levels r. (b) Variation of the proportions ρ^{A} of the aware individuals with the information level r for different information timeliness τ. In (a), $\tau = 3$. In (b), $\alpha = 0.1$. Other parameters are $\chi = 0$ in the information layer and $\delta = 0.6$ in the awareness layer. Independent activity-triggered epidemic spreading: (c) variation of the proportions of ρ^{I} the infected individuals with the epidemic infection rate β for different activity frequencies λ; (d) variation of the proportions of ρ^{I} the infected individuals with the activity frequency λ for different activity lengths κ. In (c), $\kappa = 2$. In (d), $\beta = 0.05$. Other parameters are $\theta = 0$ in the activity layer, and $\mu = 0.8$ in the epidemic layer. The data points are the results averaged over 30 MC simulations, and the corresponding color curves are the theoretical predictions of Eq. (A1) based on MMCA. Here, the same SF multiplex structure as Fig. 2 is adopted.

Incorporating with Eq. (A1), we have

$$\delta\varepsilon_i^{\mathrm{A}} = \left(1-\varepsilon_i^{\mathrm{A}}\right)\alpha\sum_{j=1}^{N}\varepsilon_j^{\mathrm{A}}a_{ji}\varphi_{ji}. \tag{A4}$$

By ignoring the second-order term $\varepsilon_i^{\mathrm{A}}\varepsilon_j^{\mathrm{A}}$, Eq. (A4) can be simplified as

$$\sum_{j=1}^{N}\left(a_{ji}\varphi_{ji} - \frac{\delta}{\alpha}e_{ji}\right)\varepsilon_j^{\mathrm{A}} = 0. \tag{A5}$$

This is an eigenvalue problem for the matrix $\mathbb{W}$, where the element w_{ji} is given by

$$w_{ji} = a_{ji}\varphi_{ji} = ra_{ji}F_{ji}(\tau,\chi) = rv_{ji}, \tag{A6}$$

where v_{ji} is the element of the matrix $\mathbb{V}$. Thus, the critical information level can be solved as

$$r_c = \frac{\delta}{\alpha\Lambda_{\max}(\mathbb{V})}, \tag{A7}$$

where $\Lambda_{\max}(\mathbb{V})$ represents the largest eigenvalue of the matrix $\mathbb{V}$. One can find that the critical information level r_c is inversely proportional to the awareness diffusion rate α, which is consistent with the simulation results in Figs. 8 and 11. Note that $\mathbb{V}$ depends on the network topology of the awareness layer, the preference of information contact, and information timeliness. As long as these are known, r_c can be explicitly solved.

APPENDIX B: INDEPENDENT ACTIVITY-TRIGGERED EPIDEMIC SPREADING

Next, we focus on the independent activity-triggered epidemic spreading when the information level is below the critical value ($r < r_c$). In this case, the spread of the epidemic is not significantly influenced by awareness diffusion. The MMCA equation for activity-triggered epidemic spreading can be approximated as

$$\rho_i^{\mathrm{I}}(t+1) = \left[1-\rho_i^{\mathrm{I}}(t)\right]\left[1-z_i(t)\right] + \rho_i^{\mathrm{I}}(t)(1-\mu). \tag{B1}$$

Figures 12(c) and 12(d) illustrate the evolution of ρ_i^{I} with β and λ. The predictions obtained from Eq. (B1) show good agreement with the numerical simulations for independent activity-triggered epidemic spreading, particularly at the epidemic threshold.

Let us now discuss the calculation of the critical activity frequency λ_c as shown in Figs. 8 and 11. To obtain λ_c, we employ a similar approach to solving r_c for independent information-driven awareness diffusion. Assuming $\rho_i^{\mathrm{I}}(t+1) = \rho_i^{\mathrm{I}}(t) = \varepsilon_i^{\mathrm{I}} \ll 1$ for $i = 1,\ldots,N$, we make the following approximation:

$$\begin{aligned} z_i &\approx \prod_{j\in\Phi_i}\left[1-\beta\varepsilon_j^{\mathrm{I}}(\sigma_{ji}+\sigma_{ij})\right] \approx 1-\beta\sum_{j\in\Phi_i}\varepsilon_j^{\mathrm{I}}(\sigma_{ji}+\sigma_{ij}) \\ &= 1-\beta\sum_{j=1}^{N}\varepsilon_j^{\mathrm{I}}b_{ji}(\sigma_{ji}+\sigma_{ij}). \end{aligned} \tag{B2}$$

By ignoring the high-order terms of ε_i^{I}, Eq. (B1) can be converted as

$$\sum_{j=1}^{N}\left[b_{ji}(\sigma_{ji}+\sigma_{ij}) - \frac{\mu}{\beta}e_{ji}\right]\varepsilon_j^{\mathrm{I}} = 0. \tag{B3}$$

Hence, the critical activity frequency λ_c can be calculated as

$$\lambda_c = \frac{\mu}{\beta\Lambda_{\max}(\mathbb{Y})}, \tag{B4}$$

where the element of the matrix $\mathbb{Y}$ is defined as $y_{ji} = b_{ji}[G_{ji}(\kappa,\theta) + G_{ij}(\kappa,\theta)]$. By knowing the network topology of the epidemic layer, preference of activity contact, and activity length, we can explicitly acquire λ_c using Eq. (B4). The simulation results presented in Figs. 8 and 11 demonstrate the effectiveness of Eq. (B4) in predicting the critical activity frequency λ_c.

[1] M. Chan-Yeung and R.-H. Xu, Sars: Epidemiology, Respirology **8**, S9 (2003).

[2] G. Neumann, T. Noda, and Y. Kawaoka, Emergence and pandemic potential of swine-origin H1N1 influenza virus, Nature (London) **459**, 931 (2009).

[3] M. Chinazzi, J. T. Davis, M. Ajelli, C. Gioannini, M. Litvinova, S. Merler, A. P. y Piontti, K. Mu, L. Rossi, K. Sun, C. Viboud, X. Xiong, H. Yu, M. E. Halloran, I. M. Longini, and A. Vespignani, The effect of travel restrictions on the spread of the 2019 novel coronavirus (COVID-19) outbreak, Science **368**, 395 (2020).

[4] K. Soltesz, F. Gustafsson, T. Timpka, J. Jaldén, C. Jidling, A. Heimerson, T. B. Schön, A. Spreco, J. Ekberg, Ö. Dahlström, F. Bagge Carlson, A. Jöud, and B. Bernhardsson, The effect of interventions on COVID-19, Nature (London) **588**, E26 (2020).

[5] R. Pastor-Satorras and A. Vespignani, Epidemic Spreading in Scale-Free Networks, Phys. Rev. Lett. **86**, 3200 (2001).

[6] R. Pastor-Satorras, C. Castellano, P. Van Mieghem, and A. Vespignani, Epidemic processes in complex networks, Rev. Mod. Phys. **87**, 925 (2015).

[7] W. Wang, M. Tang, H. E. Stanley, and L. A. Braunstein, Unification of theoretical approaches for epidemic spreading on complex networks, Rep. Prog. Phys. **80**, 036603 (2017).

[8] B. F. Nielsen, L. Simonsen, and K. Sneppen, COVID-19 Superspreading Suggests Mitigation by Social Network Modulation, Phys. Rev. Lett. **126**, 118301 (2021).

[9] L. Zeng, Y.-Q. Zeng, M. Tang, Y. Liu, Z. Liu, and Y.-C. Lai, Quantitative assessment of the effects of resource optimization and ICU admission policy on COVID-19 mortalities, Phys. Rev. Res. **4**, 033209 (2022).

[10] S. Boccaletti, V. Latora, Y. Moreno, M. Chavez, and D.-U. Hwang, Complex networks: Structure and dynamics, Phys. Rep. **424**, 175 (2006).

[11] S. Boccaletti, G. Bianconi, R. Criado, C. I. del Genio, J. Gómez-Gardeñes, M. Romance, I. Sendiña-Nadal, Z. Wang, and M. Zanin, The structure and dynamics of multilayer networks, Phys. Rep. **544**, 1 (2014).

[12] C. Castellano and R. Pastor-Satorras, Thresholds for Epidemic Spreading in Networks, Phys. Rev. Lett. **105**, 218701 (2010).

[13] M. Feng, S.-M. Cai, M. Tang, and Y.-C. Lai, Equivalence and its invalidation between non-Markovian and Markovian spreading dynamics on complex networks, Nat. Commun. **10**, 3748 (2019).

[14] L. Pan, D. Yang, W. Wang, S. Cai, T. Zhou, and Y.-C. Lai, Phase diagrams of interacting spreading dynamics in complex networks, Phys. Rev. Res. **2**, 023233 (2020).

[15] S. Zhong, X. Wu, Y. Li, and C. Liu, Indirect transmission and disinfection strategies on heterogeneous networks, Phys. Rev. E **106**, 054309 (2022).

[16] L. Han, Z. Lin, M. Tang, Y. Liu, and S. Guan, Impact of human contact patterns on epidemic spreading in time-varying networks, Phys. Rev. E **107**, 024312 (2023).

[17] N. Ferguson, Capturing human behaviour, Nature (London) **446**, 733 (2007).

[18] Z. Wang, M. A. Andrews, Z.-X. Wu, L. Wang, and C. T. Bauch, Coupled disease-behavior dynamics on complex networks: A review, Phys. Life Rev. **15**, 1 (2015).

[19] Z. Wang, C. T. Bauch, S. Bhattacharyya, A. d'Onofrio, P. Manfredi, M. Perc, N. Perra, M. Salathé, and D. Zhao, Statistical physics of vaccination, Phys. Rep. **664**, 1 (2016).

[20] S. Funk, E. Gilad, C. Watkins, and V. A. A. Jansen, The spread of awareness and its impact on epidemic outbreaks, Proc. Natl. Acad. Sci. USA **106**, 6872 (2009).

[21] M. De Domenico, A. Solé-Ribalta, E. Cozzo, M. Kivelä, Y. Moreno, M. A. Porter, S. Gómez, and A. Arenas, Mathematical Formulation of Multilayer Networks, Phys. Rev. X **3**, 041022 (2013).

[22] M. Kivelä, A. Arenas, M. Barthelemy, J. P. Gleeson, Y. Moreno, and M. A. Porter, Multilayer networks, J. Complex Netw. **2**, 203 (2014).

[23] M. De Domenico, C. Granell, M. A. Porter, and A. Arenas, The physics of spreading processes in multilayer networks, Nat. Phys. **12**, 901 (2016).

[24] C. Granell, S. Gómez, and A. Arenas, Dynamical Interplay between Awareness and Epidemic Spreading in Multiplex Networks, Phys. Rev. Lett. **111**, 128701 (2013).

[25] C. Granell, S. Gómez, and A. Arenas, Competing spreading processes on multiplex networks: Awareness and epidemics, Phys. Rev. E **90**, 012808 (2014).

[26] W. Wang, Q.-H. Liu, J. Liang, Y. Hu, and T. Zhou, Coevolution spreading in complex networks, Phys. Rep. **820**, 1 (2019).

[27] Z. Wang, Q. Guo, S. Sun, and C. Xia, The impact of awareness diffusion on SIR-like epidemics in multiplex networks, Appl. Math. Comput. **349**, 134 (2019).

[28] Y. Guo, L. Tu, H. Shen, and L. Chai, Transmission dynamics of disease spreading in multilayer networks with mass media, Phys. Rev. E **106**, 034307 (2022).

[29] H. Wang, H.-F. Zhang, P.-C. Zhu, and C. Ma, Interplay of simplicial awareness contagion and epidemic spreading on time-varying multiplex networks, Chaos **32**, 083110 (2022).

[30] Z. Wang, C. Xia, Z. Chen, and G. Chen, Epidemic propagation with positive and negative preventive information in multiplex networks, IEEE Trans. Cybern. **51**, 1454 (2021).

[31] J. Wang, W. Xiong, R. Wang, S. Cai, D. Wu, W. Wang, and X. Chen, Effects of the information-driven awareness on epidemic spreading on multiplex networks, Chaos **32**, 073123 (2022).

[32] L. Zhang, C. Guo, and M. Feng, Effect of local and global information on the dynamical interplay between awareness and epidemic transmission in multiplex networks, Chaos **32**, 083138 (2022).

[33] J. Wang, C. Yang, and B. Chen, The interplay between disease spreading and awareness diffusion in multiplex networks with activity-driven structure, Chaos **32**, 073104 (2022).

[34] X. Chang, C.-R. Cai, C.-Y. Wang, X.-S. Liu, J.-Q. Zhang, K. Jin, and W.-L. Yang, Combined effect of simplicial complexes and interlayer interaction: An example of information-epidemic dynamics on multiplex networks, Phys. Rev. Res. **5**, 013196 (2023).

[35] H. Wang, C. Chen, B. Qu, D. Li, and S. Havlin, Epidemic mitigation via awareness propagation in communication networks: The role of time scales, New J. Phys. **19**, 073039 (2017).

[36] Q. Wu and S. Chen, Coupled simultaneous evolution of disease and information on multiplex networks, Chaos Solit. Frac. **159**, 112119 (2022).

[37] T. Aoki and T. Aoyagi, Scale-Free Structures Emerging from Co-Evolution of a Network and the Distribution of a Diffusive Resource on it, Phys. Rev. Lett. **109**, 208702 (2012).

[38] H.-F. Zhang, Z.-X. Wu, M. Tang, and Y.-C. Lai, Effects of behavioral response and vaccination policy on epidemic

spreading—an approach based on evolutionary-game dynamics, Sci. Rep. **4**, 5666 (2014).

[39] L. Böttcher, O. Woolley-Meza, N. A. M. Araújo, H. J. Herrmann, and D. Helbing, Disease-induced resource constraints can trigger explosive epidemics, Sci. Rep. **5**, 16571 (2015).

[40] X. Wang, X. Zhu, X. Tao, J. Xiao, W. Wang, and Y.-C. Lai, Anomalous role of information diffusion in epidemic spreading, Phys. Rev. Res. **3**, 013157 (2021).

[41] S. Meloni, A. Arenas, and Y. Moreno, Traffic-driven epidemic spreading in finite-size scale-free networks, Proc. Natl. Acad. Sci. USA **106**, 16897 (2009).

[42] H.-X. Yang, W.-X. Wang, Y.-C. Lai, Y.-B. Xie, and B.-H. Wang, Control of epidemic spreading on complex networks by local traffic dynamics, Phys. Rev. E **84**, 045101(R) (2011).

[43] H.-X. Yang and Z.-X. Wu, Suppressing traffic-driven epidemic spreading by use of the efficient routing protocol, J. Stat. Mech.: Theory Exp. (2014) P03018.

[44] H.-X. Yang and Z. Wang, Suppressing traffic-driven epidemic spreading by adaptive routing strategy, Chaos Solit. Frac. **93**, 147 (2016).

[45] J. Chen, M.-B. Hu, and M. Li, Traffic-driven epidemic spreading in multiplex networks, Phys. Rev. E **101**, 012301 (2020).

[46] J. Chen, M.-B. Hu, Y.-H. Wu, and M. Li, Traffic-induced epidemic suppression in multiplex networks, J. Stat. Mech.: Theory Exp. (2020) 113403.

[47] M. Catanzaro, M. Boguñá, and R. Pastor-Satorras, Generation of uncorrelated random scale-free networks, Phys. Rev. E **71**, 027103 (2005).

[48] S. C. Ferreira, C. Castellano, and R. Pastor-Satorras, Epidemic thresholds of the susceptible-infected-susceptible model on networks: A comparison of numerical and theoretical results, Phys. Rev. E **86**, 041125 (2012).

[49] P. Erdős and A. Rényi, On the evolution of random graphs, Publ. Math. Inst. Hung. Acad. Sci. **5**, 17 (1960).